



Open Archive Toulouse Archive Ouverte







OATAO is an open access repository that collects the work of Toulouse researchers and makes it freely available over the web where possible

This is an author's version published in: <https://oatao.univ-toulouse.fr/26092>

Official URL:

<https://doi.org/10.1016/j.jmatprotec.2019.116452>

To cite this version:

Pasquet, Isabelle  and Baco-Carles, Valérie  and Chamelot, Pierre  and Gibilaro, Mathieu  and Massot, Laurent  and Tailhades, Philippe  A *multimaterial based on metallic copper and spinel oxide made by powder bed laser fusion: A new nanostructured material for inert anode dedicated to aluminum electrolysis*. (2020) *Journal of Materials Processing Technology*, 278. 116452. ISSN 0924-0136.

Any correspondence concerning this service should be sent to the repository administrator: tech-oatao@listes-diff.inp-toulouse.fr

A multimaterial based on metallic copper and spinel oxide made by powder bed laser fusion: A new nanostructured material for inert anode dedicated to aluminum electrolysis

I. Pasquet^a, V. Baco-Carles^a, P. Chamelot^b, M. Gibilaro^b, L. Massot^b, Ph. Tailhades^{a,*}

^a Institut Carnot Chimie Balard Cirimat, UMR CNRS 5085, Université de Toulouse, UPS-CNRS, France

^b Laboratoire de Génie Chimique, Université de Toulouse, UPS-CNRS, Toulouse, France

Keywords:

Spinel ferrite

Cermet

Nanostructuration

Additive manufacturing

Powder bed fusion

Selective laser melting

Inert anode

Coherent 3D parts of cermets, made of spinel ferrite and metallic copper, are prepared in a nitrogen atmosphere by powder bed additive manufacturing of a mixture of oxide and metallic powders. The cermets obtained are constituted by the association of blocks of about 500 μm , which create between them, a relatively large porosity (# 35%). Each block is subdivided into intimately nested zones that are either predominantly metallic or predominantly oxide type. In the metal parts, a dispersion of oxide crystals is observed, whose size varies from ten nanometers to a few micrometers. A similar distribution of metal particles in the oxide zones is also demonstrated. The chemical compositions of metallic and oxide phases are slightly different from those in the initial powders. Due to the high energy density of the laser, the melting temperature of the metal and oxides could be reached and therefore this could explain the chemical composition variations in the phases and the shape of oxide and metallic nanometric grains. The process used can therefore be described as powder bed fusion. These nanostructured cermets have been used as "inert" anodes for the electrolysis of aluminum in molten cryolite. Although penalized by a high porosity, 5 mm in diameter anodes allowed to carry out an electrolysis for 4 h. Since Spark Plasma Sintering can greatly reduce their porosity, while retaining their specific microstructure, the implementation of additive manufacturing for producing "inert" anodes is therefore of real interest.

1. Introduction

An environmental challenge for primary aluminum industry is to reduce the greenhouse gases, especially carbon dioxide, generated by the alumina electrolysis in molten cryolite baths in accordance with the Hall Heroult process. The environmental problem raised by this process is notably discussed by Hanneman et al. (1999) in the report of the American Society of Mechanical Engineers. Thonstad et al. (2008) explain the economic and technical interest of inert anodes and deal with materials that may constitute inert anodes for the electrolysis of aluminum. For many years, several studies have focused on the development of inert anodes for aluminum production that allow the release of dioxygen instead of carbon dioxide. Sadoway (2001) explains the challenges of developing inert anodes, the interest from environmental point of view and discusses advantages and drawbacks of materials such as ceramics, composites ceramic metal also called cermet and metals for this application. Pawlek (2014) takes stock of the state of the art and the evolution of research on this difficult topic. Due to their high

chemical stability, mixed spinel ferrites $\text{Ni}_x\text{Fe}_{3-x}\text{O}_4$ and/or $\text{Ni}_x\text{Co}_y\text{Fe}_{3-x-y}\text{O}_4$ ($0 < x < 1$, $0 < y < 1$) are promising materials for this application. Compositions of this type have been patented by Ray (1983) showing the importance of nickel in the chemical composition. Olsen and Thonstad (1999) emphasize the interest of anodes based on nickel ferrite. They also carry out electrolysis tests demonstrating the interest of the process. Xi et al. (2008) highlight the effect of additional elements on NiFe_2O_4 on corrosion resistance. Liu et al (2011) are particularly interested in the electrical conductivity of this family of materials and emphasize the effect of the thermal treatment on the corrosion resistance. But the electrical conductivity of spinel ferrites, usually too low, can be increased by adding a metal such as copper or a nickel copper alloy to form a ceramic metal compound also called cermet. Such materials obtained by oxidation of the surface of a copper nickel alloy and their use are described by Nguyen et al. (1990). A good protection of the anode against corrosion is however difficult to achieve by this way. Ray et al. (2001) propose an inert anode made of a bulk ceramic metal composite. The ceramic part is based on spinel ferrite

* Corresponding author.

E-mail address: tailhade@chimie.ups-tlse.fr (P. Tailhades).

containing in particular nickel. The metal comprises at least one noble metal, which increases the cost of this type of anode. A process for the selective reduction of copper in mixed ferrites predominantly substituted for copper and nickel, is also proposed by Tailhades et al. (2008), to obtain cermets for the electrolysis of aluminum. These cermets have a finer microstructure than those of their counterparts obtained by the sintering of powder mixtures. Barthelemy et al. (2016) demonstrate the value of using metal oxide composites in which the metal phase is predominant. Ceramic oxides and cermets for inert anodes are usually shaped by pressing powder after mixing with an organic binder, drying and conventional sintering. These shaping methods are described by Olsen and Thonstad (1999) and Xi et al. (2008) in the articles cited above. Variants using different binders, pressures and sintering temperatures are proposed by He et al. (2008) and Baco Carles et al. (2009). The cermets obtained by such processes, generally consist of spinel ferrites and copper (or nickel copper alloys) often associated with monoxides. The constitutive grains of these materials have sizes greater than one micrometer and more generally a few tens of micrometers as described by Barthelemy et al. (2016) or by Ray (1986). No submicron ferrite inclusions are found in the metallic phase, even in spinel ferrite cermets with the finest microstructures prepared by Baco Carles et al. (2009).

Currently, the development of powder bed additive manufacturing technologies, especially selective laser melting i.e. SLM processes, allow rapid manufacturing of three dimensional parts by melting a powder bed layer by layer. They can be implemented without any binder (direct SLM), they allow the construction of parts with complex geometry and as explained by Bourell et al. (2017), they can be applied to different materials like metals, polymers, ceramics and composites. But it is well known that high density ceramics are difficult to obtain by these technologies due to their high melting point, their low thermal conductivity, their low toughness and the short time between laser interaction and material. These difficulties are for the most part discussed by Zocca et al. (2015). In their review of laser sintering of ceramics, Qian and Shen (2013) explain the technique and also the possibility to obtain ceramic materials with new characteristics due to local high temperatures reached with laser. The porosity is used by Shishkovsky et al. (2013) to form 3D parts of oxide ceramics with perovskite or spinel structure for micro electro mechanical systems. The articles of Zocca et al. (2015) and Ferrage et al. (2017) report however, the need to improve density of ceramic parts manufactured by powder bed additive manufacturing. For this reason, Wilkes et al. (2013) suggest a preheating of the mixture of ZrO_2 Al_2O_3 to high temperature. Juste et al. (2014) also propose to add graphite in alumina powder. This process has a real efficiency but can affect the purity of the elaborated ceramics. Parameters as particle size, morphology of the powders and so powder bed density, are also very important to improve the density of the final part. This is true not only for ceramic materials, as illustrated by the work of Bertrand et al. (2007) for yttria zirconia and Danezan et al. (2018) for porcelain, but also for metals, for which the characteristics of the parts depend strongly on the quality of the feedstock, according to Tan et al. (2017). In their review, Yu et al. (2019a), also present advantages and drawbacks of different methods for nanocomposite feedstock preparation and some qualifications of the powders. However, general rules specifying the characteristics (granulometry, flowability, compaction ability ...) of the feedstock, to obtain well densified parts by an additive manufacturing process on a powder bed, have not yet been established.

The combination of spinel ferrite and metallic powders could make the build of 3D parts by powder bed additive manufacturing easier, and simultaneously, as noticed previously, improve the electrical conductivity of the material for inert anode application. In addition, the problems related to the electrical connection of the anodes or the optimization of the electrolysis processes, require sometimes electrodes with complex shapes. Such complex parts could be directly done by additive manufacturing on powder bed. This manufacturing process

would in particular prevent delicate mechanical machining for parts containing ceramic materials. Finally, conventional ceramic processes require the addition of organic binders in the shaping phases. These binders are then thermally decomposed in a neutral atmosphere so as not to oxidize the metal part. In this step, carbon oxides and toxic gaseous effluents are emitted. This step is not compatible with the environmentally friendly approach that underlies the development of inert anodes, is avoided by additive manufacturing on a powder bed.

Very recent research deal with additive manufacturing of multi materials based on powder bed fusion process and emphasize the complex microstructures obtained. Yu et al. (2019a, 2019b) provided a full review on metal matrix nanocomposites with a selective laser melting process and based on the use of nanocomposites feedstock. They describe and discuss the effect of processing parameters on density and microstructure of the final part. Koopman et al. (2019) realize a multi material made from a ZrO_2 Al_2O_3 ceramic coating on a steel substrate by a selective laser melting process. They emphasized the heterogeneous microstructure of the ceramic after the additive manufacturing.

For these reasons, the first goal of this work was to demonstrate the feasibility of coherent cermet electrodes by powder bed additive manufacturing. Another goal of this work was to compare the microstructural characteristics and phase composition of cermets, coming from this process, to those of their counterparts, obtained by conventional sintering processes. Finally, electrolytic tests in molten cryolite at 980 °C were conducted to evaluate, for the first time, the behavior of powder bed additive manufacturing cermets in such corrosive medium used for the electrolysis of alumina.

2. Materials and methods

A mixed spinel oxide was prepared by a soft chemistry route using an oxalate precursor, as summarized in Fig. 1.

A 0.55 M solution of metallic salts was prepared by dissolution of $NiSO_4$, $6H_2O$, $CoSO_4$, $7H_2O$ and $FeSO_4$, $7H_2O$ (Laurylab, 98%) in deionized water, 1% of sulfuric acid was added to prevent iron ions from oxidizing. This solution was poured with a peristaltic pump at speed of 20 mL/min, in a 0.2 M aqueous solution of ammonium oxalate ($NH_4C_2O_4$, H_2O , Laurylab, 98%) to form an oxalate precipitate,

$(Ni_xCo_yFe_{3-x-y})_{1/3}C_2O_4$, $2H_2O$. After a 30 min ageing under mechanical stirring at 300 rpm, the oxalate suspension was centrifuged. The precipitate was then washed with deionized water and dried in a ventilated oven at 80 °C.

An oxide powder was then obtained after the decomposition of the corresponding oxalate under air at 300 °C with a heating rate of 50 °C/h. A pure $Ni_xCo_yFe_{3-x-y}O_4$ spinel phase is formed at about 950 °C. But such a high temperature results in partial sintering of the grains, which

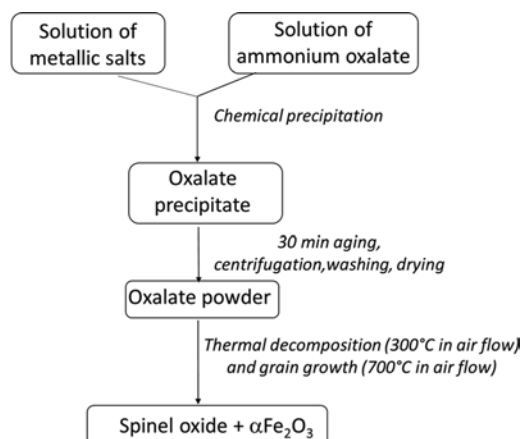


Fig. 1. Preparation of the ferrite powder.

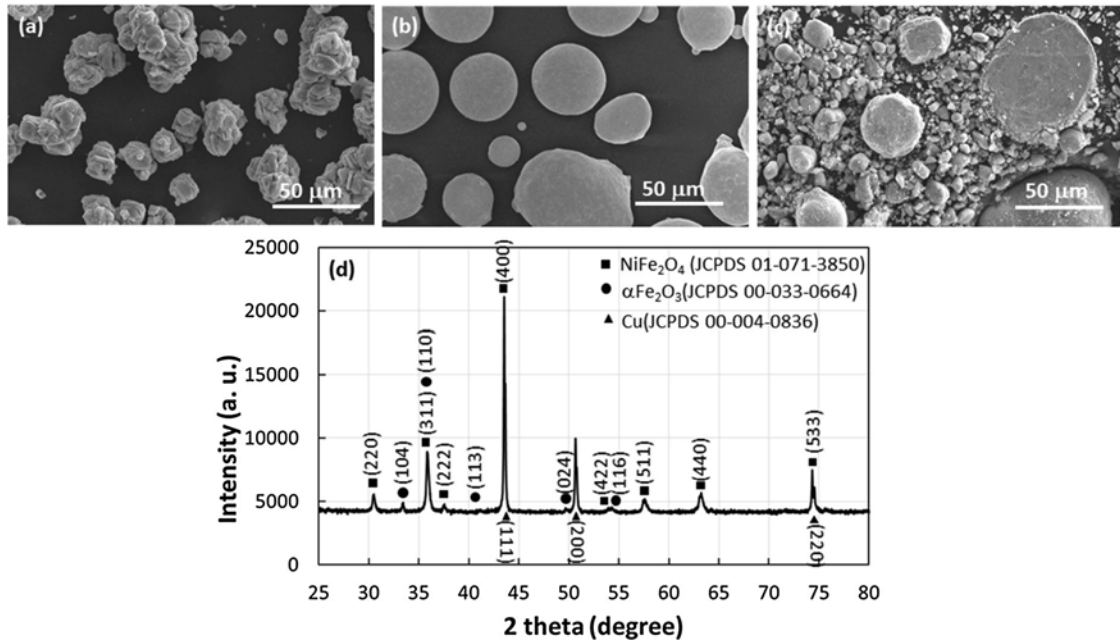


Fig. 2. Characterization of powders: scanning electron micrographs of oxide powder (a), metallic powder (b), mixture of oxide and metallic powders (c). X-ray diffractogram of the powders mixture (d).

then form aggregates of very irregular shapes and sizes. These granu-
lometric characteristics are generally unfavorable to the constitution of
a homogeneous powder bed in the additive manufacturing machine. It
was therefore decided to treat the powder at only 700 °C for one hour.
The product thus obtained is a spinel oxide in which only a very small
proportion of hematite phase remains. Moreover, the grains obtained
although polyhedral, fit fairly well into a spherical envelope and have
sizes between 10 and 15 microns, but some bigger agglomerates with
size of the order of 50 microns were also observed. These characteristics
are assumed to be compatible with the realization of powder beds
without macroscopic defect, in the additive manufacturing machine.

The atomic cationic composition of oxide powder, determined by
Inductively Coupled Plasma Atomic Emission Spectrometer (ICP AES)
analysis, was 0.24 Ni: 0.10 Co: 0.66 Fe. If the powder consists of a single
spinel phase, the ferrite is then described by the following overall for-
mula: $Ni_{0.72}Co_{0.31}Fe_{1.97}O_4$.

A commercial metallic copper powder from Goodfellow Company
was used. The morphology of particles was spherical and their size was
between 10 and 50 μm . These features are also considered compatible
with usual operation of an additive manufacturing machine. The purity
of the powder was 99%.

The oxide and metallic powders were mixed in a proportion of
37% 63 wt% respectively with a Turbula T2F mixer/shaker (WAB) for
one hour. The mixture of powders was preheated at 50 °C for 12 h just
before the powder bed manufacturing.

The real density of the mixture was measured with a helium pyc-
nometer AccuPyc II 1340 from Micromeritics. Other macroscopic char-
acteristics of the mixture were also measured to qualify its compact
ability and its rheological behavior. Measurements of apparent and
packed density and angle of repose, were thus carried out using re-
spectively, a volumeter EV02 from Electrolab Company, a jolting vo-
lometer IVO 3 from LSCI and a manual powder flow tester EFT 01
(Electrolab Company).

A ProX200 equipment from Phenix 3D System Company was used
to melt powders. This machine was equipped with a 300 W Nd:YAG
fiber laser with a 1064 nm wavelength. The laser spot was 80 μm
in diameter. The build chamber was filled with nitrogen to prevent me-
tallic copper from oxidizing and the level of O_2 was between 800 and
1000 ppm. After preliminary experiments on a steel substrate, the

thickness of the powder bed for each layer was fixed at 50 μm . The
hatch spacing was also 50 μm . No pressure was applied using the
compacting roller fitted to the additive manufacturing machine. A
raster scanning strategy with a rotation of 90 ° between the successive
layers, was applied in this study on the basis that it is commonly used
in the literature and proposed by equipment suppliers. The laser scanning
speed was 500 mm/s. The studied parameter was the power of the laser,
which varied from 45 to 100 W (i.e. in power density 9.10^5 to $19.9.10^5$
W/cm² respectively). These parameters avoid laser ablation, which has
been observed with higher power, even though it is associated with
higher scanning speed. As proposed by several authors (Liu et al., 2019;
Yu et al., 2019a, 2019b), especially to increase the density of the 3D
parts and to decrease the surface roughness, re melting was not used
in this study. Indeed, the risk was to lose the original structuration ob-
tained at a nanometric scale. Small parallelepiped parts of
 $10 \times 10 \times 1 mm^3$ were prepared for the physico chemical character-
izations and cylinders of 5 mm in diameter and 30 mm length were
manufactured and used as anodes to evaluate the behavior of the ma-
terial obtained during aluminum electrolysis in melted cryolithe.

The phase characterizations were performed by X ray diffraction
(XRD) analysis using a D4 Endeavor Bruker Diffractometer equipped
with a copper anode and a LynxEye 2D detector. The lattice parameter
of the phases was calculated by a Rietveld refinement in the Fullprof
program. The samples were also investigated by a scanning electron
microscope with a field emission gun (FEG SEM) JEOL JSM 6700 F
equipped with an energy dispersive spectrometer (EDS) Princeton
Gamma Tech. A scanning electron microscope FEI Helios600i equipped
with a focused gallium ion beam (FIB), was used to prepare thin sam-
ples for transmission electron microscopy (TEM) observations, that
were realized with a JEOL microscope JEM 2100 F fitted with a SDD
Bruker detector for EDS analysis.

A Dr Sinter 2080 machine from Sumitomo Company was used for
spark plasma sintering (SPS) experiments. The chamber was evacuated
and then filled with argon. A uniaxial pressure of 50 MPa was applied
and the current was slowly increased during the heating up to 300 A.
The sintering temperature was 800 °C to avoid the melting of copper in
the graphite mould.

3. Results

The morphology and size of the starting oxide and metallic powders and their mixture in the proportion 37 wt % oxide 63 wt % metal, are respectively presented on Fig. 2a, b and c. The X ray diffractogram of the oxide metal mixture clearly shows a spinel oxide, which displays diffraction peaks close to those of NiFe_2O_4 (JCPDS 01 071 3850) and metallic copper (JCPDS 00 004 0836). The lattice parameters of both compounds are respectively (0.8351 ± 5.10^{-4}) nm and (0.3616 ± 5.10^{-4}) nm, in agreement with that of pure $\text{Ni}_{0.72}\text{Co}_{0.31}\text{Fe}_{1.97}\text{O}_4$ powder obtained after 30 min at 1000°C (0.8345 nm) and that of JCPDS file for metallic copper. Two very small diffraction peaks can be ascribed to $\alpha\text{Fe}_2\text{O}_3$ secondary phase. This phase is due to the heat treatment of the oxide powder at 700°C only (Fig. 2d) as explained in the experimental part.

The real density measured by a helium pycnometer on the powder mixture was 7.18 g.cm^{-3} , which is close to the theoretical density for the powder mixture (7.17 g.cm^{-3}) estimated according to the following formula :

$$\rho = (\rho_{\text{Cu}} \cdot \rho_{\text{sp}}) / (p \cdot \rho_{\text{Cu}} + (1 - p) \cdot \rho_{\text{sp}}) \quad (1)$$

with : $\rho_{\text{Cu}} = 8.96 \text{ g.cm}^{-3}$, $\rho_{\text{sp}} = 5.35 \text{ g.cm}^{-3}$, p = the mass fraction of spinel ferrite.

This result obtained for different tests samples, shows the homogeneity of the mixture.

The apparent density determined on not compacted sample was 2 g.cm^{-3} after drying in an oven at 50°C for 12 h. From these measurements, the experimental indices of Hausner (packed density / apparent density) and Carr ($100 \cdot [\text{packed density} - \text{apparent density}] / [\text{packed density}]$) are close to 1.6 and 37 respectively. These values mean that the powder mixture used is of the type cohesive with a flowability (the angle of repose is close to 40 degrees) not very favorable to obtain a very dense powder bed although the grains fit fairly well into a spherical envelope and have sizes between 10 and 50 microns. A very close behavior was observed for the untreated powder at 50°C for 12 h, but spreading into homogeneous powder beds is indeed easier after such treatment that prevents the powder from sticking on the roller. In this context, it was possible to obtain powder beds without macroscopic defects by the automatic spreading system of the machine, by adjusting the thickness to 50 μm .

Taking into account the results of preliminary tests on pure copper, spinel ferrite and the mixture of both, powder bed additive manufacturing was carried out by exploring only the effect of the laser power in a limited range, for fixed scanning speeds and steps (see Methods and Materials section). Whatever the laser power applied in the range studied, parts with a surface roughness R_a close to $75 \mu\text{m}$ were obtained. The microstructure is made of well densified areas of 500 1000 micrometers in diameter (Fig. 3a) separated by pores having a size close to some hundred micrometers. The experimental real densities of the parts, simply estimated by weighing and measuring the external volume

of the samples, is at most 4.7 g.cm^{-3} . This value is much lower than that (7.18 g.cm^{-3}) measured with the helium pycnometer, on the starting powder mixture. From these data, the estimate of the relative densities of the parts after additive manufacturing process, gives values close to 65%. These values are close to those listed in the literature by Bertrand et al. (2007) for oxide parts produced by the SLS / SLM process, even if for the studied cermets, the metal tends to favor the densification as evidenced by the existence of well densified zones with high metallic content. This process does not generally make it possible to obtain well densified parts directly, the latter having to be further sintered in a furnace or in uniaxial or isostatic pressure heating setups. It was nevertheless interesting to characterize the material obtained at this stage of the process, to determine the evolution of the nature of the phases relative to the initial powder, as well as the microstructure generated by the scanning of the laser beam. This information is indeed fundamental to understand the mechanisms involved in the construction of parts by powder bed additive manufacturing.

After insolation of the powder at laser power of 45, 75, 90 or 100 W in a nitrogen atmosphere, spinel ferrite and metallic copper are identified from the XRD peaks (Fig. 3b). The parts resulting from the process therefore mainly consist of a spinel phase and metallic copper. Two other peaks of very low intensities reveal however the presence of cuprous oxide Cu_2O . However, no trace of hematite phase ($\alpha\text{Fe}_2\text{O}_3$) was detected.

Microscopic observations of the well densified areas, after samples polishing, show metallic and oxide phases in agreement with XRD. The microstructure observed after the process is however very original for each laser power used (Fig. 4). Domains consisting essentially of either a metal phase (M) or an oxide (O), are observed. The secondary electron mode was used for the images of Fig. 4 because it reveals quite well the porosity of the samples. This is very low in the metal zones (M), whatever the power applied during the manufacture of the samples. It is however more pronounced in the "oxide" (O) parts and is even more important that the laser power used is weak. The porosity is more clearly demonstrated by Fig. 5, corresponding to a sample obtained under a low laser power of 45 W ($9 \cdot 10^5 \text{ W/cm}^2$). It is indeed very visible on large areas of oxide type, but we also note that the inclusions of oxide in the metal, almost all have at least one pore within them. For the samples obtained at low laser power, certain regions are also observed in which the metal has partially penetrated the oxide through its porosity (Fig. 6). The backscattered mode of the scanning electron microscopy is, in this case, more powerful to reveal such details. For all the samples from 45 to 100 W ($9 \cdot 10^5$ to $19.9 \cdot 10^5 \text{ W/cm}^2$), the grains size is much larger than that of the initial one in the powder. Moreover, there are many inclusions of very different sizes in these grains (Figs. 4 6). Such a phase organization is encountered in all the regions of the samples, showing that there is no specific phase segregation unlike the results obtained by Martinez et al. (2019). In agreement with the previous real density measurements, this is consistent with a homogeneous starting powder mixture.

Further examination was done for a sample obtained at 90 W (17.9

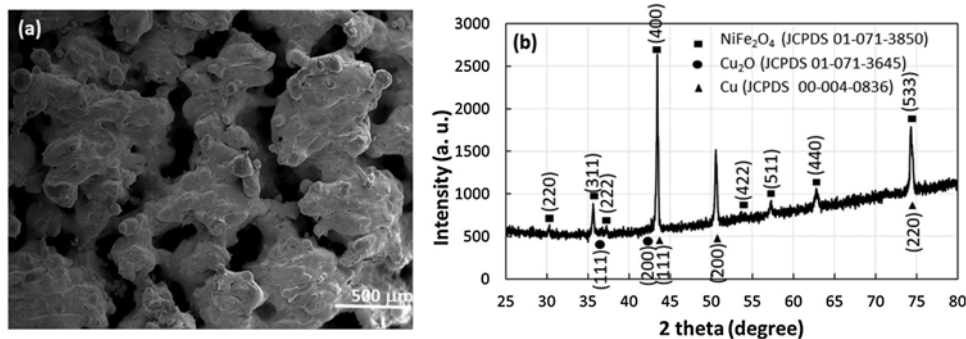


Fig. 3. SEM image of a 3D part manufactured with a laser power of 90 W (power density of $17.9 \cdot 10^5 \text{ W/cm}^2$) (a) and X-ray diffractogram of the part (b).

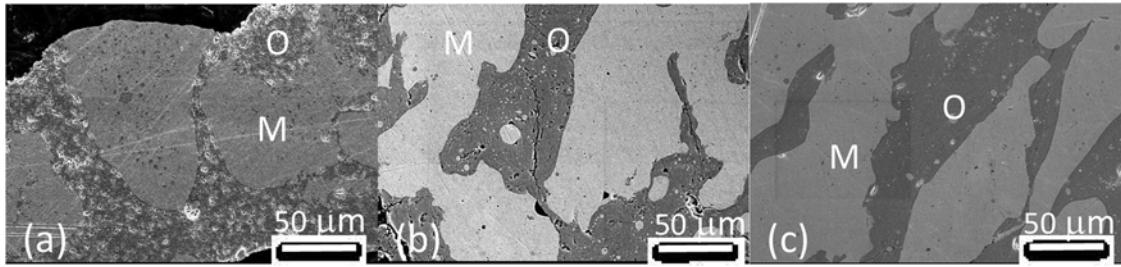


Fig. 4. Scanning electron micrographs in secondary electron mode of samples prepared at different laser powers: (a) 45 W ($9 \cdot 10^5 \text{ W/cm}^2$); (b) 75 W ($14.9 \cdot 10^5 \text{ W/cm}^2$) and c) 100 W ($19.9 \cdot 10^5 \text{ W/cm}^2$). The light (M) and dark (O) zones mainly consist of metal and ferrite, respectively.

10^5 W/cm^2) (Fig. 7). This sample was indeed one of the most interesting, especially for the subsequent electrolysis tests, given that it was a little better densified than the others and free of some cracks that can sometimes be observed when the laser power applied is higher. In the metallic zones, faceted oxide crystals, with in general a smaller structure inside, ranging in size from few nanometers to several hundred nanometers are often observed (Fig. 7c). Likewise, metal inclusions whose size dispersion is similar to that of the previous faceted crystals, appear in the large oxide zones (Fig. 7d). The sections of these metal inclusions are very often discs, suggesting that their shape is ovoid. Other morphologies sometimes appear but their contours are generally rounded and for this reason, very different from the oxide inclusions in metallic matrix.

The EDS analysis, coupled with TEM, suggests two types of small oxide particles in the metallic matrix: some in which iron, nickel, cobalt and copper too, are always detected with variable contents (Fig. 8a) and some Cu rich zone that could be a cuprous oxide. Oxide containing mainly copper was also observed close to metallic grains and sometimes around them. These regions were ascribed to the cuprous oxide detected by XRD. Copper is present in the large oxide areas, supposed to be spinel phase, at the levels of the order of 10–20 at. %. TEM micrographs also reveal very well the metallic phases (Fig. 7d) in the oxide matrix. They mostly contain copper and a small amount of nickel (less than 5 at. %) as characterized by EDS analysis (Fig. 8b).

The aim of this work was not to produce optimized materials that could be inert anodes for the electrolysis of aluminum. It was, however, to appreciate their potential with respect to this technological application, in particular their corrosion resistance under electric current when immersed in the molten cryolite. This is the reason why small cylinders (5 mm in diameter and 30 mm length) were manufactured by the additive process described above (Fig. 9), with the best laser power of 90 W, and then tested as anode during simplified tests of chemical resistance in cryolitic medium. The electrolysis bath consisted of molten cryolite salts with an addition of 5%wt of CaF_2 and 8%wt of Al_2O_3 to reach the saturation, the cryolitic ratio CR ($\text{CR} = \text{moles of NaF} / \text{moles of AlF}_3$) was closed to 2.2. Experiments were carried out at 980°C with a current density of 0.6 A/cm^2 . Electrolysis with these original but porous electrodes was possible, demonstrating a good resistance in this

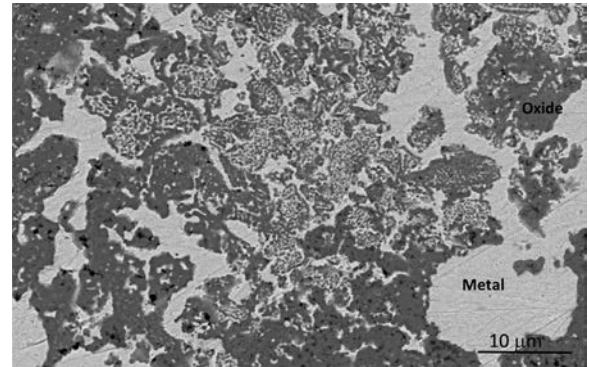


Fig. 6. Scanning electron micrographs in backscattered mode of a sample prepared at 45 W ($9 \cdot 10^5 \text{ W/cm}^2$). The oxide porosity is partially penetrated by the metal.

highly corrosive medium and a sufficient electrical conductivity. However, a significant dissolution was observed, the diameter of the electrode ranging from 5 to 2 mm in 4 h of electrolysis.

Since porosity is a factor favoring the dissolution of the samples, an evaluation of the potentialities of application to the electrolysis of aluminum, required also to ensure that it can be reduced by a post treatment.

A conventional sintering treatment was therefore implemented initially. The sintering experiment was done in nitrogen at 1060°C for 2 h in a conventional furnace for a small part of $10 \times 10 \times 1 \text{ mm}^3$ obtained by powder bed additive manufacturing. The chosen temperature was below the melting point of copper to avoid exudation during treatment. This last however didn't change the density and the microstructure of the sample, demonstrating its inefficacy to reduce the porosity at this temperature. No other experience of this type was conducted with this result in mind. The spark plasma sintering (SPS) was therefore implemented. This technique uses the combined effects of temperature, pressure and electric pulses, to facilitate sintering. As the SPS machine is also equipped with a dilatometer, it is possible to select good sintering conditions in a very short time. A temperature of 800°C and a pressure of 50 MPa, made it possible to significantly improve the

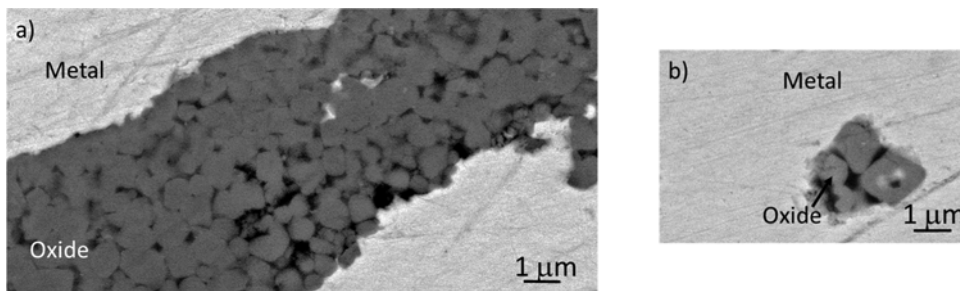


Fig. 5. Scanning electron micrographs in backscattered electron mode of a sample prepared at 45 W ($9 \cdot 10^5 \text{ W/cm}^2$). The porosity is clearly demonstrated in the large oxide zones (a) but also in the oxide inclusions in the metal (b).

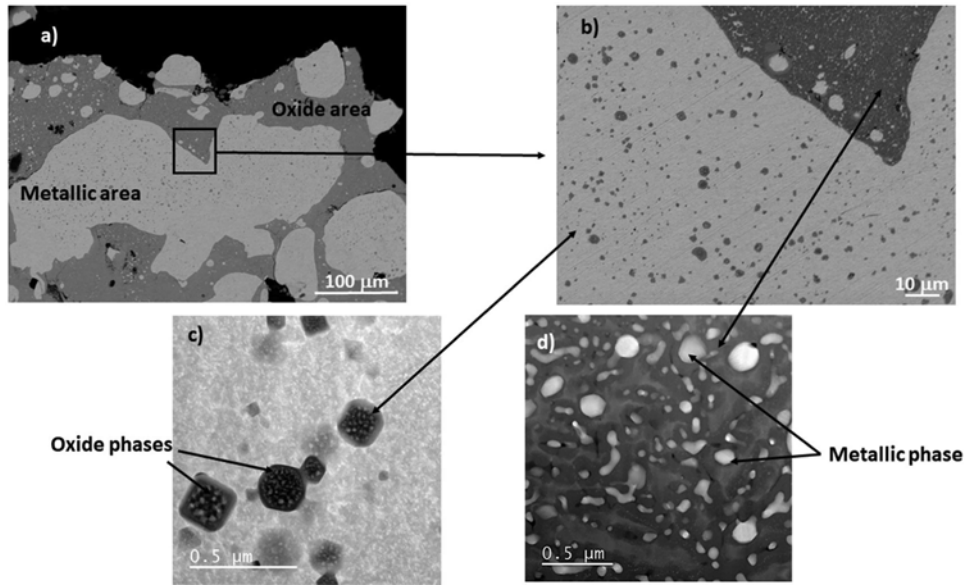


Fig. 7. Scanning electron micrographs in backscattered mode a) and b). Transmission electron micrographs in dark field of the metallic area c) and oxide area d). (Applied laser power of 90 W, i.e. power density of $17.9 \cdot 10^5 \text{ W/cm}^2$).

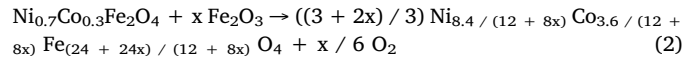
sintering, to reach a relative density greater than 90% (Fig. 10). The microstructure is therefore more compact than after forming parts by powder bed additive manufacturing, and the large metal or spinel areas and the inclusions they contain, are not fundamentally modified.

4. Discussion

The results presented above show that the manufacturing process applied to a pulverulent mixture of copper and oxide can allow the production of relatively porous but coherent cermets. Despite the existence of similar majority phases, both in the initial powder and in the pieces obtained by additive manufacturing, significant differences are noted. The latter assumes that laser irradiation has caused chemical reactions that could be interpreted as follows. The initial powder contains a spinel phase, in which the average valence state of the cations is close to 2.67 (spinel can be schematically described by the formulae $M^{2+}M_2^{3+}O_4^{2-}$ in which M^{n+} means metallic cations), and hematite ($Fe_2^{3+}O_3^{2-}$), in which the valence state of the iron is of course 3. To obtain a pure spinel phase (average valence of cations equal to 2.67) after the manufacturing process, it was therefore necessary to reduce some cations in the oxide phases, making oxygen available. This oxygen would be used for the partial oxidation of copper and so it forms copper oxide Cu_2O , as revealed by X ray diffraction. In other words, the simplified equation describing the spinel phase reduction is:



Fig. 9. Small cermet electrodes manufactured by the powder bed additive process.



The initial powder of spinel ferrite and metallic copper, is made of 37% by mass of a spinel phase close to $Ni_{0.7}Co_{0.3}Fe_2O_4$, whose molar mass is 234.5 g, and 63% by mass of metallic copper, which has an atomic mass of 63.54 g (the minority phase of hematite in the initial ferrite powder being neglected). The mixture is then made of 0.15 mol of spinel ferrite for 1 mol of metallic copper. For such a mixture, Eq. (2) indicates that the reduction of 0.15 mol of spinel ferrite generates $(0.15x / 6) O_2$ (i.e. $0.025x O_2$). This oxygen will oxidize some of the metallic copper according to:

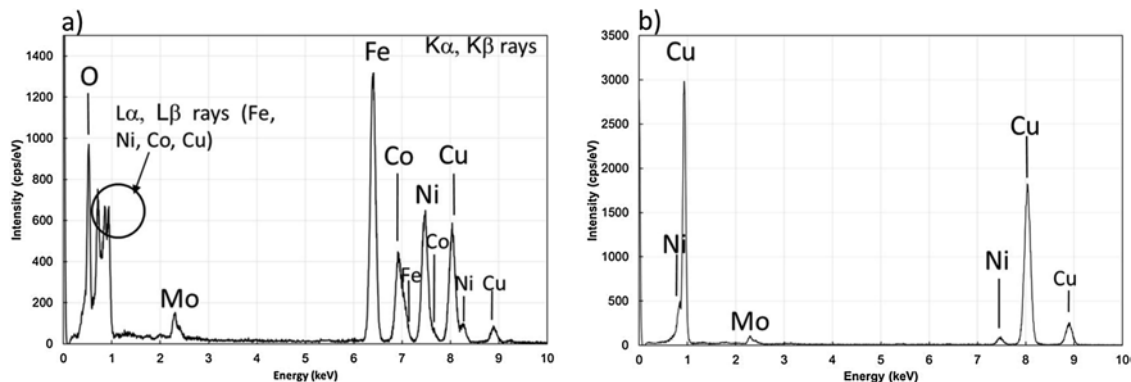


Fig. 8. Example of EDS spectra of oxide particles in metallic area (a) and metallic phase (b) (Mo signal (K α ray) is due to the grid used for thin samples preparation for TEM observations).

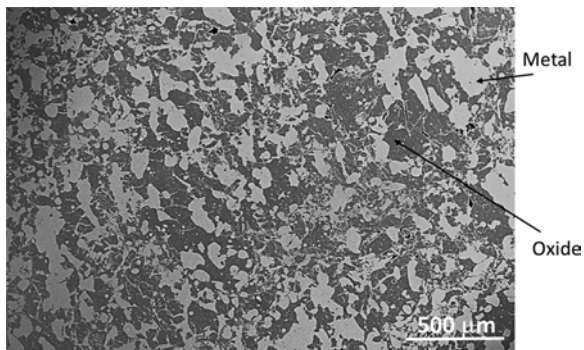


Fig. 10. Scanning electron micrograph after a post-treatment by SPS of a 3D part manufactured by SLM with a laser power of 90 W (power density of $17.9 \cdot 10^5 \text{ W/cm}^2$).



What is more surprising is the very specific microstructure of the manufactured parts, which is very different from that observed after a conventional sintering. For instance, the starting mixture of powders used for additive manufacturing experiments was pressed at 200 MPa and sintered in inert gas below or above the melting temperature of metallic copper, respectively at 1060 °C or at 1100 °C for 2 h. The observed microstructures for both sintering temperatures are similar. It is clear that the microstructure of such a sample (Fig. 11) is completely different from that of the parts from the additive manufacturing. The difference probably results from a local melting of the constituents of the material, under the strong thermal effect of the laser beam for additive process. The energy density E ($\text{J} \cdot \text{m}^{-2}$) estimated by: $E = P / (v \cdot D)$ where P is the laser power (45, 75, 90 or 100 W), v is the scan rate ($0.5 \text{ m} \cdot \text{s}^{-1}$) and D is the diameter of the laser spot ($8 \cdot 10^{-5} \text{ m}$) was between $1.13 \cdot 10^6$ and $2.5 \cdot 10^6 \text{ J} \cdot \text{m}^{-2}$ for the experiments. The highest energy densities are then of the same order than the threshold beyond which the melting of porcelain materials was reached ($2.80 \cdot 10^6 \text{ J} \cdot \text{m}^{-2}$ from Danezan et al. (2018)). Very high temperatures or local melting have also been achieved by diode laser heating of $\gamma \text{ Fe}_2\text{O}_3$ films or oxalate layers, according to the work of Bouet et al. (1999) and Pasquet et al. (2017). For the samples obtained at the lowest laser powers, the high porosity within the zones consisting mainly of oxides (Figs. 4 and 5), however suggest that the melting points of the oxides has not been reached (Melting points close to 1550–1600 °C for the mixed Ni Co Fe spinel phases). For such a small laser power, the ferrite grains of the initial powder have lost their shape, only by the action of a simple sintering in the solid state. But the high densification of the metal parts and their penetration into the porous network formed by the oxides (Fig. 6) suggests that the copper melting temperature (1083 °C) has been exceeded. The penetration of the liquid copper within the oxides is very probably the first step of the metal oxide mixture. It is then amplified by the application of stronger laser powers.

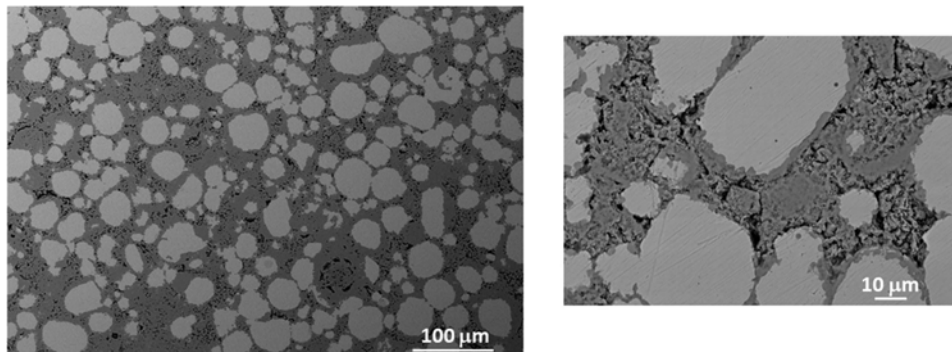


Fig. 11. Scanning electron micrographs in backscattered electron mode after a conventional sintering of the powders mixture at 1060 °C for 2 h and in an argon flow.

Moreover, the application of high laser powers also seems to cause the fusion of the oxide zones. These become in fact strongly densified. The more intimate metal oxide mixture that is found elsewhere, could also be the result of the mixing at the liquid state of the different constituents of the material. In this hypothesis, the rapid cooling following laser irradiation, should first lead to the solidification of the oxide, having the highest melting point, then that of the metal. The images of Fig. 7c seem consistent with such a process, because they show many faceted and symmetrical oxide crystals within a metal matrix, as if the crystallization was made in a liquid, so in the absence of a strong mechanical stress. In large areas of spinel ferrite, the droplets of molten metal are trapped by the crystallization of the matrix. As the cooling continues, the metal solidifies in the space that the spinel phase left and then cannot freely develop its crystalline faces. The metal thus adopts the ovoid or vermicular form that it had in the liquid state. In a simplified manner, the manufacturing process involves the changes schematically described in Fig. 12, to finally obtain the original microstructure of the cermet.

For the reasons mentioned above and in particular the melting and mixing of oxide or metal constituents, the samples from the powder bed additive manufacturing do not retain the memory of the particle size of the initial powder mixture, unlike conventional sintering. The latter gives rise to a microstructure in which metal grains were found, whose size (10 to 50 μm) has not significantly changed compared to that they had in the powder mixture. It just seems that they were trapped in the spinel matrix under the effect of sintering. For such a sample, the EDS analysis shows that metallic phase contains only copper. About 2% of copper is found in the spinel oxide in which iron, cobalt and nickel are in the same proportion than in the starting powder. Due to the very low copper content in the spinel ferrite, its lattice parameter is not different from that of the powder. Small particles (200 nm) of oxide or metal, were sometimes observed in metallic and oxide zones respectively. However, such inclusions are rare and have a very different average size and size distribution that for the cermet obtained by additive manufacturing. All these observations confirm that the diffusion phenomena are much smaller in the conventional sintering process at about 1000–1100 °C and that it does not allow a phase mixture as intimate as that obtained after additive manufacturing. The local temperature reached during the additive manufacturing process at high laser power, estimated at more than 1550 °C, about 500 °C above the temperature chosen for the conventional elaboration of the cermet, is the main reason for this difference ($T(\text{Additive manufacturing}) \geq 1550 \text{ °C}$, $T(\text{conventional sintering}) = 1060 \text{ °C}$). In fact, for the conventional sintering, only local solid-solid reactions are possible while the additive manufacturing process involves phenomena of diffusion and convection in the liquid state that affect the material more strongly.

One of the objectives of the present work was also to demonstrate the feasibility by the additive manufacturing process of cermet type electrodes of complex composition. Then, their use as inert anode for the aluminum production was tested. The goal was to verify the cermet

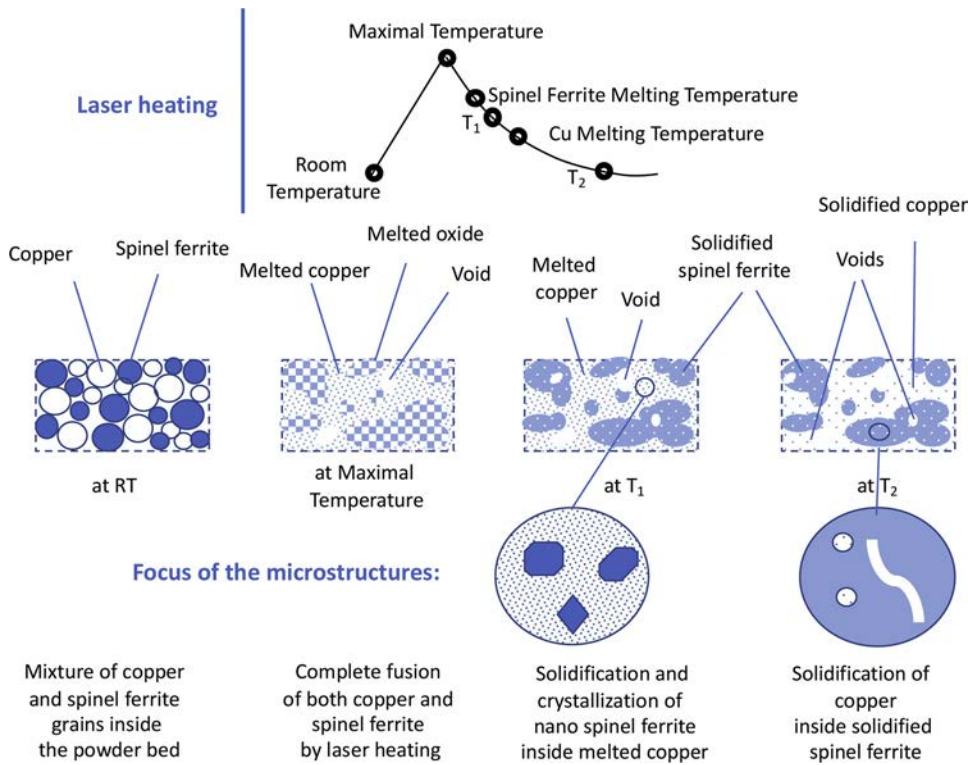


Fig. 12. Simplified microstructural evolution under high power laser heating: the initial powder bed is melted by the laser spot, the oxide and the metal are partially mixed in the molten medium, voids are formed due to the porosity of the bed of initial powder. Once cooled, the spinel ferrite is solidified first and nanocrystals are formed inside the molten copper. At low temperatures, the copper solidifies. Spherical or vermicular copper particles can be observed inside the ferrite cavities.

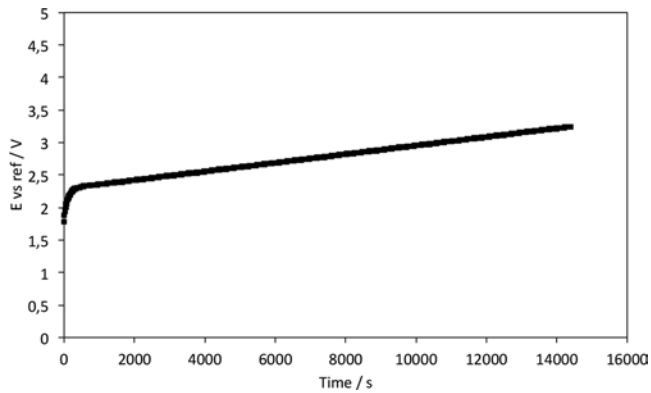


Fig. 13. Anode potential versus time for the metal-oxide electrode obtained by additive manufacturing with a laser power of 90 W ($17.9 \cdot 10^5 \text{ W/cm}^2$).

anode stability under electrolysis and the oxygen release on such material. The experiment was performed under industrial conditions (Hall Héroult process) with cryolitic medium (Na_3AlF_6) melted at 980°C and intensiostatic electrolysis at 0.6 A/cm^2 for 4 h. A 5 mm diameter cermet anode was used and the electrolysis curve (anode potential versus time) is presented in Fig. 13. A good stability in the time is observed at a potential corresponding to the O_2 evolution as mentioned by Oudot et al. (2014). This promising behavior could be further improved by reducing the open porosity that reaches a high value ($\approx 35\%$) with the sample studied. This evolution seems possible because, as shown previously, additional SPS sintering makes it possible to leave a porosity of only a few percent, without modifying the specific microstructure generated by the additive manufacturing. It will therefore be interesting in a future work, to test such densified electrodes and to compare their behavior in term of corrosion resistance, with those obtained by conventional sintering. The technological applications of additive manufacturing could then be expanded if such a comparison was significantly favorable to the samples that would come from it.

5. Conclusion

In this work, coherent but porous 3D cermet parts, based on spinel ferrites and metallic copper, were manufactured by a SLM process for the first time. This study revealed a very original microstructure of the cermet parts whatever the manufacturing parameters. Indeed the SLM process allowed to create a nanostructured material from a micrometric powders mixture while maintaining a spinel oxide and a metal as main phases. However, the phase compositions were slightly different from those of the initial powders. Microstructure and changes in phase composition could be due to the local melting of the compounds involved by the high temperatures reached under a focused laser beam. The porosity of the parts was a major defect for alumina electrolysis in melted cryolite. A first electrolysis under industrial conditions (Hall Héroult process) with cryolitic medium (Na_3AlF_6) melted at 980°C and intensiostatic electrolysis at 0.6 A/cm^2 for 4 h, with an electrode of 5 mm in diameter, was however performed on this material. Because it is possible to correct defect due to porosity by an additional spark plasma sintering, improvement in corrosion resistance could be expected. Moreover, the microstructural specificities induced by additive manufacturing can be retained after such a sintering technique.

For the future, the combinations of process parameters should be refined in order to know if it is possible to directly obtain highly densified cermets and thus simplify the production process. Given their number, these combinations have not all been studied. A systematic exploration of the effect of pitch (hatch spacing) and the speed of laser spot seems to be particularly important. The scanning strategy and laser re melting could also be studied to improve the surface roughness and density of the as build part. The other line of work consists of conducting an electrolysis test campaign on electrodes issued from conventional sintering process and the most densified samples, obtained directly or after SPS. From these experiments, the influence of the specific microstructure of the samples from the additive manufacturing, on the performances under electrolysis conditions, could be determined and the reasons for possible favorable effects could be better understood. These results would also make it possible to approach optimal performances of the cermets studied, for the application to inert anodes.

At this stage, the addition of the traditional advantages of laser assisted powder bed fusion, to the possibility of obtaining original materials by their microstructure, could lead to a positive decision on the future of this manufacturing method, in the field of aluminum electrolysis. A new industrial application would then open for SLM technology.

Moreover, original cermets with ferrimagnetic oxides such as spinel ferrites, are interesting to make new magnetic materials to meet the ever increasing demands of electrical systems and machinery.

Acknowledgements

This work was supported by the French ANR program ANR 13 RMNP 012 and the MultiFab project (Occitanie Region and Fond Européen de Développement Régional). The authors particularly thank V. Baylac and G. Chevalier, Université de Toulouse, for respectively manufacturing 3D parts by SLM and sintering samples by SPS. The authors acknowledge S. Dulaud, Université de Toulouse, for TEM preparation and characterization at UMS Castaing and Professor Didier Beziat GET Laboratory (UMR CNRS 5563) for helpful discussions.

References

- Baco-Carles, V., Pasquet, I., Laurent, V., Gabriel, A., Tailhades, Ph., 2009. Preparation and dense micro-cermets made of nickel ferrite and metallic copper. *Solid State Sci.* 11, 1503–1506.
- Barthelemy, C., Marmottant, A., Laurent, V., Bouvet, S., Stabrowski, V., 2016. Cermet Electrode Material. WO 2016/156973 A1. .
- Bertrand, Ph., Bayle, F., Combe, C., Goeuriot, P., Smurov, I., 2007. Ceramics components manufacturing by selective laser sintering. *Appl. Surf. Sci.* 254, 989–992.
- Bouet, L., Tailhades, Ph., Pasquet, I., Bonningue, C., Le Brun, S., Rousset, A., 1999. Cation-deficient spinel ferrites: applications for high-density write-once optical recording. *Jpn. J. Appl. Phys.* 38, 1826–1828.
- Bourell, D., Kruth, J.P., Leu, M., Levy, G., Rosen, D., Beese, A.M., 2017. Materials for additive manufacturing. *Manuf. Technol.* 66, 659–681.
- Danezan, A., Delaizir, G., Teyssier-Doyen, N., Gasgnier, G., Gaillard, J.M., Dupont, P., Nait-Ali, B., 2018. Selective laser sintering of porcelain. *J. Eur. Ceram. Soc.* 38, 769–775.
- Ferrage, L., Bertrand, G., Lenormand, P., Grossin, D., Ben-Nissan, B., 2017. A review of the additive manufacturing (3DP) of bioceramics : alumina, zirconia (PSZ) and hydroxyapatite. *J. Aust. Ceram. Soc.* 53, 11–20.
- Hanneman, R.E., Hayden, H.W., Goodnow, W., et al., 1999. Report of the American Society of Mechanical Engineers'. Technical Working Group on Inert Anode Technologies. ASME International.
- He, H., Zhou, K., Li, Z., Huang, B., 2008. Effect of BaO addition on electric conductivity of xCu/10NiO-NiFe₂O₄ cermets. *Trans. Nonferrous Met. Soc. China.* 18, 1134–1138.
- Juste, E., Petit, F., Lardot, V., Cambier, F., 2014. Shaping of ceramic parts by selective laser melting of powder bed. *J. Mater. Res.* 29, 2086–2094.
- Koopman, J., Voigt, J., Niendorf, T., 2019. Additive manufacturing of a steel-ceramic multi-material by selective laser melting. *Metall. Mater. Trans. B.* 50 (2), 1042–1051.
- Liu, B., Zhang, L., Zhou, K., Li, Z., Wang, H., 2011. Electrical conductivity and molten salt corrosion behavior of spinel nickel ferrite. *Solid State Sci.* 13, 1483–1487.
- Liu, B., Li, B.Q., Li, Z., 2019. Selective laser remelting of an additive layer manufacturing process on AlSi10Mg. *Results Phys.* 12, 982–988.
- Martinez, R., Todd, I., Mumtaz, K., 2019. In situ alloying of elemental Al-Cu12 feedstock using selective laser melting. *Virtual Phys. Prototyp.* 14 (3), 242–252.
- Nguyen, T., Lazouni, A., Doan, K. S., 1990. Ceramic/Metal composite material. US Patent 4,960,494.
- Olsen, E., Thonstad, J., 1999. Nickel ferrite as inert anodes in aluminium electrolysis : part 1 material fabrication and preliminary testing. *J. Appl. Electrochem.* 29, 293–299.
- Oudot, M., Cassayre, L., Chamelot, P., Gibilaro, M., Massot, L., Pijolat, M., Bouvet, S., 2014. Layer growth mechanisms on metallic electrodes under anodic polarization in cryolite alumina melt. *Corros. Sci.* 79, 159–168.
- Pasquet, I., Le Trong, H., Baco-Carles, V., Presmanes, L., Bonningue, C., Baylac, V., Tailhades, Ph., Conedera, V., Calmon, P.F., Dragomirescu, D., Camon, H., 2017. Direct shaping of oxides by laser insolation of transition metal oxalates. *J. Eur. Ceram. Soc.* 37, 5315–5320.
- Pawlek, R.P., 2014. Inert anodes: an update. *Light Metals.* Grandfield J, Springer Cham, pp. 1309–1313.
- Qian, B., Shen, Z., 2013. Laser sintering of ceramics. *J. Asian Ceram. Soc.* 1, 315–321.
- Ray, S. P., 1983. Composition for inert electrodes. US Patent 4,399,008.
- Ray, S. P., 1986. Inert electrode composition having agent for controlling oxide growth on electrode made therefrom. US Patent 4,582,585.
- Ray, S. P., Liu, X., Weirauch Jr, D. A., 2001. Electrolytic production of high purity aluminum using inert anodes. US Patent 6,217,739 B1.
- Sadoway, D.R., 2001. Inert anodes for the Hall-Heroult cell: the ultimate materials challenge. *JOM* 53, 34–35.
- Shishkovsky, I., Morozov, Y., Kuznetsov, M., 2013. Layering fabrication, structure, and electromagnetic properties of perovskite phases and hybrid process: self-propagated high-temperature synthesis and selective laser sintering. *Phase Transit. A Multinatl. J.* 86, 1085–1093.
- Tailhades, Ph., Rousset, A., Gabriel, A., Laurent, V., Baco-Carles, V., Lamaze, A. P., 2008. Inert anode for the production of aluminum by fused bath electrolysis and method of making this anode. US Patent 7,425,284 B2.
- Tan, J.H., Wong, W.L.E., Dalgarno, K.W., 2017. An overview of powder granulometry on feedstock and part performance in the selective laser melting process. *Addit. Manuf.* 18, 228–255.
- Thonstad, J., Galasiu, I., Galasiu, R., 2008. Inert anodes for aluminium electrolysis. *Molten Salts.* 93, 1–4.
- Wilkes, J., Hagedorn, Y.C., Meiners, W., Wissenbach, K., 2013. Additive manufacturing of ZrO₂-Al₂O₃ ceramic components by selective laser melting. *Rapid Prototyp. J.* 19, 51–57.
- Xi, J., Xie, Y., Yao, G., Liu, Y., 2008. Effect of additive on corrosion resistance of NiFe₂O₄ ceramics as inert anodes. *Trans. Nonferrous Met. Soc. China.* 18, 356–360.
- Yu, W.H., Sing, S.L., Chua, C.K., Kuo, C.N., Tian, X.L., 2019a. Particle-reinforced metal matrix nanocomposites fabricated by selective laser melting : a state of the art review. *Prog. Mater. Sci.* 104, 330–379.
- Yu, W.H., Sing, S.L., Chua, C.K., Kuo, C.N., Tian, X.L., 2019b. Influence of re-melting on surface roughness and porosity of AlSi10Mg parts fabricated by selective laser melting. *J. Alloys. Compd.* 792, 574–581.
- Zocca, A., Colombo, P., Gomes, C.M., Günster, J., 2015. Additive of manufacturing ceramics : issues, potentialities, and opportunities. *J. Am. Ceram. Soc.* 98, 1983–2001.